bioRxiv preprint doi: https://doi.org/10.1101/738310; this version posted August 17, 2019. The copyright holder for this preprint (which was not certified by peer review) is the author/funder, who has granted bioRxiv a license to display the preprint in perpetuity. It is made available under aCC-BY-NC 4.0 International license.

Modelling geospatial distributions of the triatomine vectors of *Trypanosoma cruzi* in Latin America

Andreas Bender[1¤*], Andre Python[1], Steve W. Lindsay[2], Nick Golding[3], Catherine L Moyes[1*]

1 Big Data Institute, Li Ka Shing Centre for Health Information and Discovery, University of Oxford, Old Road Campus, Oxford, UK
2 Department of Biosciences, Durham University, DH1 3LE, Durham, UK
3 Department of BioSciences,University of Melbourne, Parkville, Melbourne, Victoria, Australia.

¤Big Data Institute, Li Ka Shing Centre for Health Information and Discovery, University of Oxford, Old Road Campus, Oxford, UK
* bender.at.research@gmail.com, catherinemoyes@gmail.com

Abstract

Approximately 150 triatomine species are known to be infected with the Chagas parasite, *Trypanosoma cruzi*, but they differ in the risk they pose to human populations. The largest risk comes from species that have a domestic life cycle and these species have been targeted by indoor residual spraying campaigns, which have been successful in many locations. It is now important to consider residual transmission that may be linked to persistent populations of dominant vectors, or to secondary or minor vectors. The aim of this project was to define the geographical distributions of the community of triatomine species in Latin America. Presence-only data with over 12,000 observations of triatomine vectors were extracted from a public database and target-group background data were generated to account for sampling bias in the presence data. Geostatistical regression was then applied to estimate species distributions and fine-scale distribution maps were generated for thirty triatomine vector species. The results for *Panstrongylus geniculatus*, *P. megistus*, *Triatoma barberi*, *T. brasiliensis*, and *T. pseudomaculata* are presented in detail and the model validation results for each of the 30 species are presented in full. The predictive maps for all species are made publicly available so that they can be used to assess the communities of vectors present within different regions of the endemic zone. The maps are presented alongside key indicators for the capacity of each species to transmit *T. cruzi* to humans. These indicators include infection prevalence, evidence for human blood meals, and colonisation or invasion of homes. A summary of these indicators shows that the majority of the 30 species mapped by this study have the potential to transmit *T. cruzi* to humans.

Author summary

The Pan American Health Organisation's Strategy and Plan of Action for Chagas Disease Prevention, Control and Care highlights the importance of eliminating those triatomine vector species that colonise homes, and has had great success in many locations. Since indoor residual spraying campaigns have targeted these species, their importance relative to other vectors has diminished and their geographical distributions

bioRxiv preprint doi: https://doi.org/10.1101/738310; this version posted August 17, 2019. The copyright holder for this preprint (which was not certified by peer review) is the author/funder, who has granted bioRxiv a license to display the preprint in perpetuity. It is made available under aCC-BY-NC 4.0 International license.

may also have changed. It is now vital to consider the full community of vector species, including previously dominant vectors as well as secondary or minor vector species, in order to target residual transmission to humans. Our aim was to define the geographical distributions of the most commonly reported triatomine species in Latin America. We extracted reports of triatomine vector species observed at specific locations from a public database and we used a geostatistical model to generate fine-scale predictive maps for thirty triatomine vector species. We present these maps alongside a summary of key indicators related to the capacity of each species to transmit the Chagas parasite to humans. We show that most of the 30 species that we have mapped pose a potential threat to human populations.

Introduction

American trypanosomiasis, or Chagas disease, is one of the 10 neglected diseases addressed by the London Declaration, which calls for control and elimination of these devastating diseases by 2020 [1]. It is a disease of Latin America and the Pan American Health Organisation (PAHO) has set out a 'Strategy and Plan of Action for Chagas Disease Prevention, Control and Care' [2]. This strategy includes the elimination of domestic vectors to prevent intra-domiciliary transmission, as well as screening blood donors and pregnant women to prevent transmission via blood donation or the placenta, and implementation of best practice in food handling to prevent oral transmission. Our study focuses on the primary route of infection; the contamination of a vector bite by the faeces of that vector.

The *T. cruzi* parasite is transmitted to humans by over 150 different vector species from 18 different genera [3]. The transmission risk that each vector species poses is influenced by how likely it is to come into contact with humans and this, in turn, is influenced by short-distance movement (for example does the species enter and/or colonise homes) and its larger-scale geographical distribution. Studies assessing vulnerability of individuals to Chagas disease have shown that, while housing, ecotype and soci-economics are all relevant, triatomine presence is the most important indicator [4]. Thus understanding the distribution of these vector species is vital to both target control measures and to assess disease risk.

Before the current intervention era, five vector species were recognised as being dominant in the transmission of *Trypanosoma cruzi* to humans based on their habit of colonising houses, behaviour (feeding-defecation interval) and widespread geographical distributions [5]. Since indoor residual spraying (IRS) campaigns have successfully targeted these dominant species in many locations, their importance relative to other vectors has diminished and their geographical distributions may also have changed [6]. It is now vital to understand the full community of vector species, including previously dominant vectors as well as secondary or minor vector species, in order to target residual transmission to humans [6–8]. Data on intervention coverage with spatially and temporally high resolution across the entire zone was, however, unavailable and thus could not be taken into account at the modelling stage.

Several studies have investigated species behaviours that influence short distance travel in and around homes, such as host-seeking, aggregation and dispersal [9–19], but fewer studies have considered the larger-scale geographical distributions of these species. The studies of geographical species distributions that have been conducted typically focus on a single country or a region within a country [19–24]. One earlier study considered the distribution of infected vectors across South America, without distinguishing species [25], but no studies have considered the geographical distributions of individual dominant and secondary vector species in Latin America. A lack of consistent region-wide information makes it harder to construct an overview for the

bioRxiv preprint doi: https://doi.org/10.1101/738310; this version posted August 17, 2019. The copyright holder for this preprint (which was not certified by peer review) is the author/funder, who has granted bioRxiv a license to display the preprint in perpetuity. It is made available under aCC-BY-NC 4.0 International license.

region as a whole or to compare areas within the endemic zone.

The data recording presence of a species are often sparse and suffer from sampling bias, which makes inter-region comparison of these records difficult. The aim of this study is to use statistical models to produce a comprehensive set of maps predicting the distributions of triatomine vector species while taking into account the limitations of the data. We use an extensive database of reported occurrences of each species, data on environmental variables that are likely to influence species presence, and build species distribution models to improve our current understanding of the spatial distribution of *T. cruzi*.

Materials and methods

Species occurrence and background points

The primary source of vector species data was a database of vector occurrence locations, which was supplemented with additional species presence points derived from a database of infections in vector species. Data on vector occurrence were extracted from DataTri, a publicly available database that reports the presence of a given triatomine species, the date of collection (if available) and geographical coordinates for each collection [26]. Additional vector occurrence data was added using a database of *Trypanosoma cruzi* infections in triatomines that also provided the vector species found, the date of collection (if available) and geographical coordinates for each collection [27]. Any data points from DataTri that were duplicated in the second data set were removed before vector occurrence data from the infections database were added to the DataTri data set. Data points before the year 2000 were removed because the aim was to investigate vector distributions in the current era.

The available vector occurrence data is usually referred to as *presence only* data. Techniques for modelling such data often involve augmenting the presence data with *pseudo-absence* or *background* points, which requires a source of appropriate background data [28–30]. Here we use a target-group background (TGB) approach by choosing background data that exhibits similar sampling bias as the occurrence data [31]. This approach can reduce the bias introduced by preferential sampling of the presence locations. It was successfully used to map geographical distributions of malaria hosts and vectors [32] and predict infection risk zones of yellow fever [33]. In simulation studies this method also performed well when compared to approaches using presence-absence data [31, 34]. As with all models of presence-only data, the maps produced using the TGB approach represent relative rather than absolute probabilities of species occurrence.

We constructed one TGB data set for each vector species as outlined below and illustrated in Figure 1 for *Panstrongylus megistus*:

(1) The presence locations of vector species $k = 1, \ldots, K$ (target-group) were extracted from the database and a convex hull containing all presence locations was constructed (panel (A) in Figure 1).
(2) This hull was extended by a constant width of 5 degrees in all directions to allow for uncertainty with respect to the range of the species being modelled (*extended hull*; panel (B) in Figure 1).
(3) The presence locations of all other species within the extended hull were defined as background points (blue dots in panel (C) of Figure 1).
(4) Duplicate observations at the same site and the same year were removed.
(5) At the modelling stage, the background points were weighted such that their total weight is equal to the number of presence observations (cf. [31, 32]).

bioRxiv preprint doi: https://doi.org/10.1101/738310; this version posted August 17, 2019. The copyright holder for this preprint (which was not certified by peer review) is the author/funder, who has granted bioRxiv a license to display the preprint in perpetuity. It is made available under aCC-BY-NC 4.0 International license.

For some species, only few observations were available in the data set. It was suggested that approximately five [35] or ten [36–38] events (presences) per predictor are required to reliably fit a logistic regression. Given that we use up to 30 predictors, this would imply a sample size of $n \approx 150$ and ≈ 300, respectively. In our data, 14 and and 9 species fulfilled this (approximate) requirement. For completeness, we fit models for all species with $n > 50$, but obviously results must be interpreted with care as the sample size (number of presence observations) decreases (see Results section). Species with fewer than fifty observations in the training and test data were not modelled, however, their presence locations were used as background points for the species that were modelled.

Fig 1. Construction of background points. Illustration of the construction of background points using the TGB approach for species *Panstrongylus megistus*. Panel (A): A convex hull is constructed around the presence locations of the species. Panel (B): The hull is extended by a fixed width of 5 degrees (*extended hull*). Panel (C): Background points are added using presence locations of all other species within the extended hull. Panel (D): Blocks of width w_k are allocated randomly across the extended hull. The observations in blocks numbered 1-4 are used as training data, and the observations in blocks numbered 5 are assigned to the test data. One fold consists of all blocks sharing the same number.

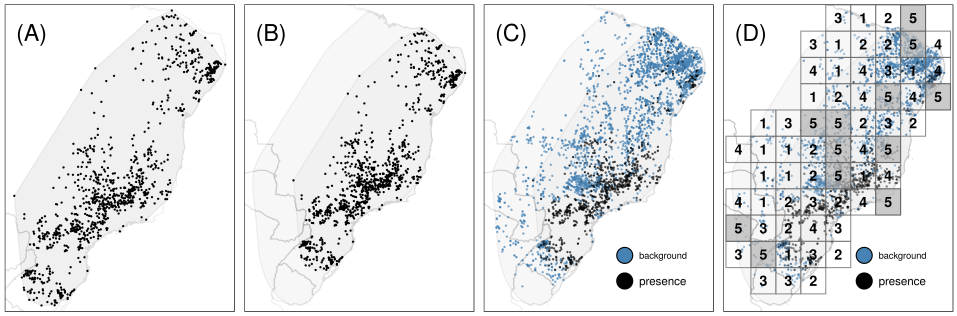

Environmental variables

Previous work has shown that vector distributions are influenced by climate, land cover types and rural/urban classifications [19–24]. Environmental variables for these three data types were obtained at a nominal resolution of 5×5 kilometres. The climatic variables used were *land surface temperature* (annual; day, night and diurnal difference) [39], two measures of *surface moisture* (annual) [40], *rainfall* (annual) [41], *elevation* (static) [42] and *slope* (static) [43]. The variable used for land cover were the 16 IGBP *land cover* classes (annual) [44] and an *enhanced vegetation index* [45]. Finally the variables used to distinguish rural, peri-urban and urban areas were *urban footprint* (static) [46], *nighttimelights* (static) [47], *human population* (annual) [48] and *accessibility* (static, based on road networks and distance to cities) [49]). Annual environmental variables were not always available for all time periods in which occurrence data was available. In this case, we instead used values from the closest year.

Model evaluation

In the context of spatial analysis, data available for modelling often only encompasses few locations in areas for which predictions are generated. Therefore, the model is usually evaluated on out of sample data to avoid over-fitting, to ensure transferability to new locations and to obtain realistic estimates for the goodness of fit. Standard

bioRxiv preprint doi: https://doi.org/10.1101/738310; this version posted August 17, 2019. The copyright holder for this preprint (which was not certified by peer review) is the author/funder, who has granted bioRxiv a license to display the preprint in perpetuity. It is made available under aCC-BY-NC 4.0 International license.

approaches to model evaluation, however, can yield over-optimistic metrics of the model predictive ability unless the spatial nature of the data (and the model) is taken into account [50–52]. To address these concerns, the data was initially split randomly into *train-test data* (80%) and *evaluation data* (20%), stratified by species. The latter data set is only used for the final model evaluation, without ever being used for estimation (column "AUC*" in Table 2). Additionally, the train-test data was split into five folds. Following recommendations in [53] each fold consisted of multiple spatial blocks, where the block size w_k for species $k = 1, \ldots, K$ was set such that approximately 50 blocks (10 per fold) would cover the extended hull of that species and defined as $w_k = \sqrt{\frac{a_k}{50}}$, where a_k is the area of the extended hull of species $k = 1, \ldots, K$. Figure 1 (panel (D)) depicts the resulting blocks and folds for species *Panstrongylus megistus*. For each species, blocks one through four were assigned to the training data, while blocks numbered five (grey shade) were only used to obtain out-of-sample test errors. Allocation of blocks was spatially random to avoid systematic bias of presence and background locations in any of the folds, but stratified with respect to species presence such that the proportion of presence and background points was approximately equal in all folds. The spatial blocking for all species considered in our analyses are provided in the supplement (S1 File). Model performance was evaluated by the area under the receiver operator curve (AUC), which measures the models ability to discriminate between presence and background points.

Modelling

Let $\mathcal{E}_k \in \mathbb{R}^2$ the extended hull of species $k = 1, \ldots, K$ and $y_{k,t,i} \in \{0, 1\} \sim Bernoulli(\pi_{k,t,i}),\ i = 1, \ldots, n_k$ the binary indicator of presence/background for species k in year $t \in \{2000, \ldots, 2016\}$ at location $s_i \in \mathcal{E}_k$ (as constructed by the TGB approach). The relative probability of occurrence $\pi_{k,t,i}$ is estimated by a logistic generalised additive model (GAM) with linear predictor (1)

$$\eta_{k,t,i} = \log\left(\frac{\pi_{k,t,i}}{1 - \pi_{k,t,i}}\right) = \beta_0 + \sum_{p=1}^{P_k} f_{k,p}(x_{p,t,i}) + GP_{k,i}(\ell), \quad i = 1, \ldots, n_k, \qquad (1)$$

where $f_{k,p}(x_{p,t,i})$ is the species specific, potentially non-linear, effect of the p-th covariate estimated by a penalised thin-plate spline [54] and $GP_{k,i}(\ell)$ is a two-dimensional, species specific Gaussian process (GP) with range parameter ℓ evaluated at location s_i (the smoothness parameter was set to 1.5). The number of covariates P_k can vary by species as some of them might not have enough unique values within the spatial extent of the species to be relevant for analysis. Here, covariates were only included if the number of unique values was at least twenty. The correlation function of the GP was defined by $C(x, x') = \rho(||x - x'||)$, where $\rho(d) = (1 + d/\ell)\exp(-d/\ell)$ is the simplified Matérn correlation function with range parameter $\ell = max_{ij}||x_i - x_j||$ as suggested in [55] and implemented in [56].

The model was estimated by optimising the penalised restricted maximum likelihood (REML) criterion (2)

$$D(\boldsymbol{\psi}) + \gamma(\phi(\boldsymbol{\psi}) + \phi^*(\boldsymbol{\psi})) \qquad (2)$$

using a double shrinkage approach where $\boldsymbol{\psi}$ is a vector of all coefficients associated with the smooth functions f and GP, $D(\boldsymbol{\psi})$ is the model deviance and $\phi(\cdot)$ and $\phi^*(\cdot)$ are range space and null space penalties of the model coefficients $\boldsymbol{\psi}$ [54, 57]. The first penalty (range space) controls the smoothness of functions $f_{k,p}$ and GP_k, while the second penalty (null space) enables the removal of individual terms from the model entirely. The γ parameter can be used to globally increase the penalty and thus to

bioRxiv preprint doi: https://doi.org/10.1101/738310; this version posted August 17, 2019. The copyright holder for this preprint (which was not certified by peer review) is the author/funder, who has granted bioRxiv a license to display the preprint in perpetuity. It is made available under aCC-BY-NC 4.0 International license.

obtain smoother, sparser and therefore potentially more robust models. Practical estimation was performed using techniques introduced in [58, 59] to increase computational speed and reduce memory requirements.

Six model specifications (Table 1) were considered for this analysis, varying by the definition of covariate effects in Equation 1 and whether the global GP term $GP_{k,i}(\ell)$ was included. For each species, the final model (out of the six candidate models in Table 1) was selected based on its performance (AUC) on the test data (fold 5). Model 1 has no tuning parameters and was fit directly to the complete training data (folds 1-4). Models 2 through 6 were first tuned with respect to the global penalty $\gamma \in \{1, \ldots, 4\}$ based on 4-fold cross-validation on folds 1 through 4. Based on the value of γ that yielded the highest average AUC, the models were refit on the complete training data. All models were estimated using methods described in [60] to reduce run time and memory load.

Table 1. Model specifications considered in the analysis.

Model specification	Covariate effect definition	GP (global)
1	linear effects $f_{k,p}(x_p) := \beta_{k,p} \cdot x_p$	No
2		Yes
3	$f_{k,p}(x_p) := \sum_{m=1}^{10} B_{p,m}(x_p)\psi_{k,p,m}$, where $B_{p,m}(x_p)$	No
4	and $\psi_{k,p,m}$ are spline basis functions and coefficients	Yes
5	spatial (bivariate) varying coefficient model	No
6	$f_{k,p}(x_p) := GP_{k,p}(\ell) \cdot x_p$	Yes

Implementation

All calculations were performed using the **R** language environment [61]. Thematic maps were created using package **tmap** [62]. Data munging and pre-processing was performed using packages **dplyr** [63] and **tidyr** [64]. Spatial cross-validation was set up using package **blockCV** [65]. Package **mgcv** was used to fit the GAMs [56].

Vectorial capacity of the mapped species

For each triatomine species that was mapped, information related to its importance in transmitting *T. cruzi* to humans was collated. The prevalence of infection with the *T. cruzi* parasite was calculated using the data from an existing repository [27]. Collections of less than twenty individuals of a species were excluded and the mean prevalence was calculated for all species where the remaining number of collections exceeded ten. Relevant behavioural data for each vector species was extracted from the literature.

Results

Species Distribution

A total of 30 species were mapped. A summary for all species that were modelled is provided in Table 2, including the specification of the model selected on training data as well as the AUC of this model evaluated on test data (fold 5) and the AUC obtained on the 20% randomly selected hold-out data (denoted by AUC*). The former is an indicator of the model's transferability and ability to predict into new areas with potentially unseen covariate values or combinations, within the area that was modelled

bioRxiv preprint doi: https://doi.org/10.1101/738310; this version posted August 17, 2019. The copyright holder for this preprint (which was not certified by peer review) is the author/funder, who has granted bioRxiv a license to display the preprint in perpetuity. It is made available under aCC-BY-NC 4.0 International license.

(cf. Figure 1). The latter value indicates how well the model interpolates as indicated by its ability to predict data points not used during model training and selection.

Maps for six example species, highlighting different genera, geographical ranges, dominant vector status and behaviours, are given in Figure 2. These are *Panstrongylus geniculatus*, *Panstrongylus megistus*, *Triatoma barberi*, *Triatoma brasiliensis*, *Triatoma infestans* and *Triatoma pseudomaculata*. Maps (including 95% CI) for all species listed in Table 2 are given in the supplement (S2 File, `.gri` file format). Respective visualisations are available from S3 File. The AUC values were all well above the 0.5 random classification threshold (mean: 0.85, SD: 0.12), indicating the maps usefulness to identify areas of higher probability of presence relative to background points. The comparatively low AUC values for species *T. brasiliensis* and *T. pseudomaculata* could be partially due to an overlap with many other species, thus making it difficult to discriminate between presence and background. The AUC* values were on average higher and had a lower variance (mean: 0.88, SD: 0.08) but generally consistent with the AUC values obtained on the test data (fold 5).

Fig 2. Predicted relative probability of occurrence at every 5×5 km pixel within the respective extended hull of species occurrence.

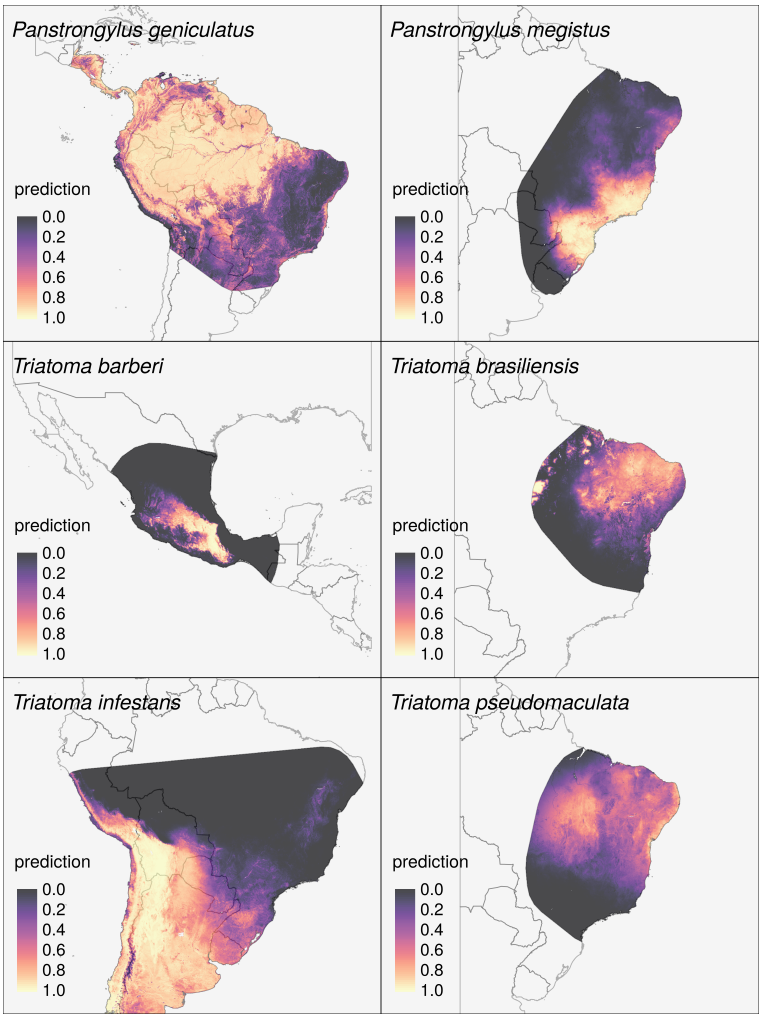

bioRxiv preprint doi: https://doi.org/10.1101/738310; this version posted August 17, 2019. The copyright holder for this preprint (which was not certified by peer review) is the author/funder, who has granted bioRxiv a license to display the preprint in perpetuity. It is made available under aCC-BY-NC 4.0 International license.

The map for *T. brasiliensis* highlights some regions with potentially suitable habitats at the north and north-west of the extended hull, however, these regions were rarely sampled, containing neither presence nor background points and should be considered uncertain (cf. maps of lower and upper 95% confidence intervals in supplement S3 File). *T. infestans* presence locations on the other hand are mostly located close to the Andes with only a few background observations in the vicinity of these locations. The predictive map (Figure 2, bottom left panel) indicates a high probability of occurrence at high altitudes. This concurs with other studies that reported *T. infestans* presence in high altitudes [66, 67], however, difficult access means that the density of sampling points is often reduced in high altitude areas, which, in turn, exhibit higher uncertainty in the predictions.

Vectorial capacity of the mapped species

The current state of knowledge on factors related to the capacity of each of the mapped species to transmit *T. cruzi* to humans (vectorial capacity) is summarised in Table 3. Specifically, mean infection prevalence, confirmation of human blood meals in natural vector populations, and confirmation of colonisation or invasion of homes (including in urban areas) are listed. Less information is available on the feeding-defecation interval or defecation location for each species, and these values may be influenced by the different experimental conditions used, so these variables are not included in Table 3 but sources of evidence are listed in File S4. The 30 most commonly reported species mapped here encompass the five most important dominant vectors that frequently colonise homes (*P. megistus*, *R. prolixus*, *T. brasiliensis*, *T. dimidiata* and *T. infestans*) as well as species that often colonise peridomestic habitats such as chicken coops, rats nests, boundary walls, wood piles, palm trees, and livestock housing. These species encompass a range of mean *T. cruzi* infection prevalences from 0.8 % in *T. sordida* to 55.6 % in *T. longipennis*, although for 13 of the most commonly reported species there was insufficient data to generate a reliable mean infection prevalence value. When viewing the summaries in Table 3, it is important to note that not all regions or species have been sampled or tested equally and a lack of published evidence for a specific component of vectorial capacity cannot be taken as definitive evidence of its absence. For example, no infections have been reported in *Eratyrus mucronatus* or *Psammolestes tertius*, but only 28 and 143 individuals have been tested, respectively, compared to 335,467 *T. sordida* individuals. In addition to the five important dominant vectors, there is evidence that many of the species mapped in this work are potential vectors of *T. cruzi*. Almost all of the 28 species that have been found to be infected with *T. cruzi* are known to invade homes, and at least 17 have been found to have fed on humans (Table 3). The sources of evidence — 126 published articles in total — are given in supplement File S4.

Data availability

Original data sources for the construction of species occurrence and background data are publicly available from [26] and [27]. The predicted maps (rasters, i.e. the predicted values for every pixel) for all 30 species in Table 2 as well as the respective lower and upper bounds of the confidence intervals are available from [68] (S2 File). Visualisations of these data, i.e. map images, are available from supplement S3 File). The code for the analysis is available at `https://github.com/adibender/chagas-vector-sdm`. Since the occurrence data and covariate data cannot be accessed programmatically, this code provides full methodological details, but cannot be used to reproduce the entire analysis.

bioRxiv preprint doi: https://doi.org/10.1101/738310; this version posted August 17, 2019. The copyright holder for this preprint (which was not certified by peer review) is the author/funder, who has granted bioRxiv a license to display the preprint in perpetuity. It is made available under aCC-BY-NC 4.0 International license.

Table 2. Summary table for all species considered in the analysis ordered by number of presence observations.

species	n presence (test)	n background (test)	Selected model (γ)	AUC	AUC*
Triatoma infestans	2499 (430)	4458 (896)	5 (3)	0.96	0.97
*Triatoma dimidiata**	1186 (154)	2883 (787)	6 (4)	0.97	0.93
Panstrongylus megistus	968 (213)	3409 (827)	6 (1)	0.83	0.89
Triatoma brasiliensis	820 (151)	1989 (346)	2 (1)	0.69	0.81
*Triatoma sordida**	809 (139)	4919 (768)	5 (2)	0.83	0.89
Triatoma pseudomaculata	804 (239)	3100 (687)	4 (1)	0.73	0.81
Triatoma barberi	455 (56)	2161 (612)	4 (1)	0.88	0.92
Triatoma mexicana	430 (44)	2046 (456)	6 (2)	0.92	0.96
Rhodnius prolixus	319 (42)	962 (229)	4 (2)	0.64	0.85
Panstrongylus geniculatus	282 (39)	6425 (824)	3 (1)	0.87	0.82
*Triatoma longipennis**	282 (25)	1974 (324)	2 (2)	0.97	0.95
Triatoma gerstaeckeri	280 (91)	2480 (482)	2 (1)	0.85	0.96
Triatoma protracta	269 (42)	2092 (212)	6 (1)	0.89	0.97
*Triatoma pallidipennis**	256 (15)	2286 (265)	2 (2)	0.96	0.96
Panstrongylus lutzi	136 (8)	2965 (609)	1 (–)	0.78	0.92
Rhodnius pictipes	130 (25)	3542 (940)	5 (1)	0.91	0.91
Triatoma rubida	126 (23)	1913 (388)	4 (1)	0.98	0.95
Rhodnius neglectus	122 (18)	3993 (655)	4 (1)	0.93	0.95
*Triatoma mazzottii**	105 (7)	2531 (581)	4 (1)	0.8	–
Rhodnius pallescens	93 (21)	898 (202)	2 (1)	0.78	0.89
*Triatoma guasayana**	92 (8)	2761 (493)	1 (–)	0.52	0.75
Triatoma rubrovaria	92 (11)	572 (227)	3 (1)	1.00	0.95
Rhodnius robustus	90 (22)	3395 (915)	4 (1)	0.97	0.94
Triatoma sanguisuga	89 (17)	701 (173)	5 (2)	1.00	0.92
Psammolestes tertius	75 (17)	3969 (825)	2 (3)	0.79	0.90
*Eratyrus mucronatus**	67 (13)	2495 (656)	5 (4)	0.80	0.84
Triatoma maculata	65 (10)	907 (169)	5 (3)	0.8	0.80
Panstrongylus chinai	57 (7)	209 (53)	4 (1)	0.8	–
Rhodnius nasutus	56 (10)	2178 (423)	2 (1)	0.90	0.83
*Panstrongylus rufotuberculatus**	55 (13)	3262 (608)	3 (3)	0.66	0.61

Summary table for thirty species for which predictive maps were created, ordered by number of occurrence observations. Species highlighted in bold are shown in Figure 2, maps of all 30 species (including 95% CI) are given in the supplement (S2 File and S3 File). Asterisks (*) mark species for which the block width w_k used to construct spatial blocking was smaller than a preliminary estimation of the range of spatial auto-correlation, thus estimated AUC values might be overoptimistic in these cases. Column "Selected model" indicates the model specification that was selected based on its performance on the training data and refers to the model specifications defined in Table 1. If applicable, γ indicates the value of the selected global penalty multiplier (cf. Eq. (2)). The reported AUC value was calculated on the test data set (fold 5 in Figure 1). The AUC* value was calculated on the 20% hold-out data (not spatially blocked). Entries "–" indicate that there were not enough observations and/or unique predicted values in the hold-out data for calculation.

bioRxiv preprint doi: https://doi.org/10.1101/738310; this version posted August 17, 2019. The copyright holder for this preprint (which was not certified by peer review) is the author/funder, who has granted bioRxiv a license to display the preprint in perpetuity. It is made available under aCC-BY-NC 4.0 International license.

Table 3. Infection prevalence and behaviour of selected species.

Species	Mean percent infected (n)	Human blood meals	Colonises homes	Invades home	Urban areas
Eratyrus mucronatus	NIF	-	yes	yes	-
Panstrongylus chinai	yes	-	yes	yes	-
Panstrongylus geniculatus	7.6 (46)	yes	-	yes	yes
Panstrongylus lutzi	6.8 (27)	yes	-	yes	-
Panstrongylus megistus	8.3 (261)	yes	yes	yes	yes
Panstrongylus rufotuberculatus	yes	-	yes	yes	-
Psammolestes tertius	NIF	-	-	-	-
Rhodnius nasutus	8.5 (73)	-	-	yes	-
Rhodnius neglectus	4.0 (120)	yes	-	yes	yes
Rhodnius pallescens	yes	yes	-	yes	-
Rhodnius prolixus	9.0 (10)	yes	yes	yes	-
Rhodnius pictipes	24.6 (36)	yes	-	yes	yes
Rhodnius robustus	25.9 (19)	-	-	yes	-
Triatoma barberi	yes	-	yes	yes	yes
Triatoma brasiliensis	3.2 (918)	yes	yes	yes	-
Triatoma dimidiata	28.9 (24)	yes	yes	yes	-.
Triatoma gerstaeckeri	yes	yes	yes	yes	-
Triatoma guasayana	yes	yes	-	yes	-
Triatoma infestans	27.6 (61)	yes	yes	yes	-
Triatoma longipennis	55.6 (14)	-	yes	yes	yes
Triatoma maculata	18.4 (18)	yes	-	yes	yes
Triatoma mazzottii	yes	-	-	yes	-
Triatoma mexicana	yes	-	-	yes	-
Triatoma pallidipennis	4.8 (17)	yes	yes	yes	yes
Triatoma protracta	yes	-	yes	yes	yes
Triatoma pseudomaculata	2.7 (988)	yes	yes	yes	yes
Triatoma rubida	yes	-	yes	yes	yes
Triatoma rubrovaria	3.1 (17)	-	-	yes	yes
Triatoma sanguisuga	yes	yes	-	yes	yes
Triatoma sordida	0.8 (1407)	yes	yes	yes	yes

The mean infection prevalence is given together with the number of triatomine collections that contributed to the mean. If there were insufficient data to calculate the mean, i.e. fewer than 10 collections of ≥ 20 individuals, then records of infected individuals (yes) or no infections found (NIF) are noted. Instances where there was no evidence for a particular behaviour are denoted by "-" .

bioRxiv preprint doi: https://doi.org/10.1101/738310; this version posted August 17, 2019. The copyright holder for this preprint (which was not certified by peer review) is the author/funder, who has granted bioRxiv a license to display the preprint in perpetuity. It is made available under aCC-BY-NC 4.0 International license.

Discussion

This study models the contemporary geospatial distributions of the thirty most commonly reported triatomine species and putative vectors of the *T. cruzi* parasite to humans. Our approach allows the distributions of these different species to be compared, and to be overlaid, which increases our understanding of the community of vector species at different locations in the current intervention era.

Our aim was to consider the most commonly reported species in Latin America. To provide policy makers, stakeholders and researchers with relevant information, we included all species for which distribution maps could be reasonably estimated. However, as can be seen from Table 2, the training (and test) data for many species contained fewer than 300 or even fewer than than 150 presence observations reported since the year 2000. For some of these species, the test fold (cf. Table 2) only contained a few presence locations, sometimes concentrated in a few blocks, i.e., within a small geographical area. AUC values will thus tend to be less robust and potentially over- or under optimistic as sample size decreases. One should therefore be particularly cautious when interpreting results of species with few presence data points and always take into account the uncertainty of the estimates as presented in the supplement (S3 File). There are locally important species for which maps could not be produced because they are only found within areas where the relevant surveillance records are not publicly available or because their range is limited so only small numbers of observations exist. For example, *Rhodnius ecuadoriensis* is an important vector in Ecuador [69] but the databases used in this study only provided 11 and 23 records, respectively, for known collection dates after the year 2000.

Earlier studies [19, 20, 22, 23, 25], most notably [24], have modelled the distributions of some of these species but only in specific regions, states or countries. Additionally, comparisons with the previous work are limited because of differences in methodology, data sets and spatial extent under consideration. Only visual comparison is possible in most cases because the predicted values generated by other studies are not openly available, precluding quantitative assessment of the different versions. In general, our respective predicted maps show very good agreement with respect to regions that highlight higher vs. lower probabilities of occurrence, but often differ with respect to the spatial extent of the region modelled.

The maps generated by this study should be considered in the context of the behaviour and vectorial capacity of each species. Summaries of the available evidence are provided here and show that most of these species are potentially important vectors of *T. cruzi* to humans. Each of the indicators of vectorial capacity summarised at a species level by this study may vary within the range of the species, as well as between species [70, 71]. It is therefore important to map spatial variation in these characteristics, as well as in the species themselves, in order to identify where regions of vectorial transmission risk are likely to exist.

bioRxiv preprint doi: https://doi.org/10.1101/738310; this version posted August 17, 2019. The copyright holder for this preprint (which was not certified by peer review) is the author/funder, who has granted bioRxiv a license to display the preprint in perpetuity. It is made available under aCC-BY-NC 4.0 International license.

Supporting information

S1 File. Presence/background data and spatial blocking.
This file contains one figure for each species contained in Table 2. In each figure, the left panel shows raw presence absence data constructed as described in Figure 1, panels (A) through (C). Panel (D) shows the spatial allocation of blocks that define training (folds 1-4) and test (fold 5) data. The figures are published in [72] and available from `https://figshare.com/s/f027db53093230373fa5`.

S2 File Predicted 5×5 km resolution maps (raw).
Files in `.gri` format that contain the predicted relative probability of occurrence for 30 traitomine species (Chagas vectors). The files consist of the predicted probabilities (`predicted-maps-tgb.gri`) and the respective lower (`predicted-cil-tgb.gri`) and upper (`predcited-ciu-tgb.gri`) confidence intervals. Each layer in the raster brick represents one species. The files are published in [68] and available from `https://figshare.com/s/78e2c83427772ddd6cc9`.

The data can be read into **R** using command `raster::brick`. For example:

```
# read in predcitions for all 30 species
pred_maps <- raster::brick("predicted-maps-tgb.grd")
# visualise prediction for species Panstrongylus megistus
sp::plot(pred_maps[["Panstrongylus.megistus"]])
```

S3 File. Predicted 5×5 km resolution maps (visualisation).
This file contains one figure for each species contained in Table 2 depicting the predicted relative probabilities of occurrence for each species. In each figure, the left and right panel show the lower and upper bound of the 95% confidence interval, respectively. The middle panel the expected value. The file is published in [73] and available from `https://figshare.com/s/ffeeb36f30dc6c128819`.

S4 File. Sources of evidence for variables linked to vectorial capacity.
This file contains the full information summarised in Table 3 together with citations for the sources of evidence used. The file is available from `https://figshare.com/s/3dd02aa5a969aefb08ad`.

Acknowledgements

This work was funded by a Bill & Melinda Gates Foundation grant (OPP1053338) to S.W.L. and a Wellcome grant (108440/Z/15/Z) to C.L.M.

bioRxiv preprint doi: https://doi.org/10.1101/738310; this version posted August 17, 2019. The copyright holder for this preprint (which was not certified by peer review) is the author/funder, who has granted bioRxiv a license to display the preprint in perpetuity. It is made available under aCC-BY-NC 4.0 International license.

References

1. London Declaration on Neglected Tropical Diseases. 5 Feb 2019; 2012.

2. Pan American Health Organization. Strategy and plan of action for Chagas disease prevention, control and care; 2010.

3. World Health Organization. Chagas disease in Latin America: an epidemiological update based on 2010 estimates. Weekly Epidemiological Record. 2015;90:33–44.

4. Montenegro D, da Cunha AP, Ladeia-Andrade S, Vera M, Pedroso M, Junqueira A. Multi-criteria decision analysis and spatial statistic: an approach to determining human vulnerability to vector transmission of *Trypanosoma cruzi*. Memorias Do Instituto Oswaldo Cruz. 2017;112(10):709–718.

5. Guhl F. Geographical distribution of Chagas Disease. In: Telleria J, Tibayrenc M, editors. American Trypanosomiasis Chagas Disease: One Hundred Years of Research; 2017. p. 89–106.

6. Buitrago R, Bosseno MF, Depickere S, Waleckx E, Salas R, Aliaga C, et al. Blood meal sources of wild and domestic *Triatoma infestans* (*Hemiptera*: *Reduviidae*) in Bolivia: connectivity between cycles of transmission of *Trypanosoma cruzi*. Parasites & Vectors. 2016;9:214.

7. Hernandez C, Salazar C, Brochero H, Teheran A, Stella Buitrago L, Vera M, et al. Untangling the transmission dynamics of primary and secondary vectors of *Trypanosoma cruzi* in Colombia: parasite infection, feeding sources and discrete typing units. Parasites & Vectors. 2016;9:620.

8. Cantillo-Barraza O, Garces E, Gomez-Palacio A, Cortes LA, Pereira A, Marcet PL, et al. Eco-epidemiological study of an endemic Chagas disease region in northern Colombia reveals the importance of *Triatoma maculata* (*Hemiptera*: *Reduviidae*), dogs and *Didelphis marsupialis* in *Trypanosoma cruzi* maintenance. Parasites & Vectors. 2015;8:482.

9. Indacochea A, Gard CC, Hansen IA, Pierce J, Romero A. Short-Range Responses of the Kissing Bug *Triatoma rubida* (*Hemiptera*: *Reduviidae*) to Carbon Dioxide, Moisture, and Artificial Light. Insects. 2017;8(3).

10. Weinberg D, Porcasi X, Lanfri S, Abril M, Scavuzzo CM. Spatial analyzes of triatomine infestation indices and their association to the actions of a Chagas disease program and environmental variables during a 5-year intervention period. Acta Tropica. 2018;188:41–49.

11. Dantas ES, Gurgel-Goncalves R, Maciel Villela DA, Monteiro FA, Maciel-de Freitas R. Should I stay or should I go? Movement of adult *Triatoma sordida* within the peridomestic area of a typical Brazilian Cerrado rural household. Parasites & Vectors. 2018;11.

12. Flores A, Vitek C, Feria-Arroyo TP, Fredensborg BL. Temporal Variation in the Abundance and Timing of daily Activity of Chagas Disease Vector *Triatoma gerstaeckeri* (Stal, 1859) in a natural Habitat in the lower Rio Grande Valley, South Texas. Journal of Parasitology. 2017;103(5):574–578.

13. Di Iorio O, Gurtler RE. Seasonality and temperature-dependent Flight Dispersal of *Triatoma infestans* (*Hemiptera*: *Reduviidae*) and Other Vectors of Chagas Disease in Western Argentina. Journal of Medical Entomology. 2017;54(5):1285–1292.

bioRxiv preprint doi: https://doi.org/10.1101/738310; this version posted August 17, 2019. The copyright holder for this preprint (which was not certified by peer review) is the author/funder, who has granted bioRxiv a license to display the preprint in perpetuity. It is made available under aCC-BY-NC 4.0 International license.

14. Brito RN, Goria DE, Diotaiuti L, Gomes ACF, Souza RCM, Abad-Franch F. Drivers of house invasion by sylvatic Chagas disease vectors in the Amazon-Cerrado transition: A multi-year, state-wide assessment of municipality-aggregated surveillance data. PLoS Neglected Tropical Diseases. 2017;11(11).

15. Falvo ML, Figueiras ANL, Manrique G. Spatio-temporal analysis of the role of faecal depositions in aggregation behaviour of the triatomine *Rhodnius prolixus*. Physiological Entomology. 2016;41(1):24–30.

16. Dias JVL, Queiroz DRM, Martins HR, Gorla DE, Pires HHR, Diotaiuti L. Spatial distribution of triatomines in domiciles of an urban area of the Brazilian Southeast Region. Memorias Do Instituto Oswaldo Cruz. 2016;111(1):43–50.

17. Jacome-Pinilla D, Hincapie-Penaloza E, Ortiz MI, David Ramirez J, Guhl F, Molina J. Risks associated with dispersive nocturnal flights of sylvatic *Triatominae* to artificial lights in a model house in the northeastern plains of Colombia. Parasites & Vectors. 2015;8.

18. Castillo-Neyra R, Barbu CM, Salazar R, Borrini K, Naquira C, Levy MZ. Host-Seeking Behavior and Dispersal of *Triatoma infestans*, a Vector of Chagas Disease, under Semi-field Conditions. PLoS Neglected Tropical Diseases. 2015;9(1).

19. Curtis-Robles R, Hamer SA, Lane S, Levy MZ, Hamer GL. Bionomics and Spatial Distribution of Triatomine Vectors of *Trypanosoma cruzi* in Texas and Other Southern States, USA. American Journal of Tropical Medicine and Hygiene. 2018;98(1):113–121.

20. Parra-Henao G, Suarez-Escudero LC, Gonzalez-Caro S. Potential Distribution of Chagas Disease Vectors (*Hemiptera*, *Reduviidae*, *Triatominae*) in Colombia, Based on Ecological Niche Modeling. Journal of Tropical Medicine. 2016;.

21. Ceccarelli S, Rabinovich JE. Global Climate Change Effects on Venezuela's Vulnerability to Chagas Disease is Linked to the Geographic Distribution of Five Triatomine Species. Journal of Medical Entomology. 2015;52(6):1333–1343.

22. Hernandez J, Nunez I, Bacigalupo A, Cattan PE. Modeling the spatial distribution of Chagas disease vectors using environmental variables and people's knowledge. International Journal of Health Geographics. 2013;12.

23. Garza M, Arroyo TPF, Casillas EA, Sanchez-Cordero V, Rivaldi CL, Sarkar S. Projected Future Distributions of Vectors of *Trypanosoma cruzi* in North America under Climate Change Scenarios. PLoS Neglected Tropical Diseases. 2014;8(5).

24. Ramsey JM, Peterson AT, Carmona-Castro O, Moo-Llanes DA, Nakazawa Y, Butrick M, et al. Atlas of Mexican *Triatominae* (*Reduviidae*: *Hemiptera*) and vector transmission of Chagas disease. Memorias Do Instituto Oswaldo Cruz. 2015;110(3):339–352.

25. Ceccarelli S, Balsalobre A, Susevich ML, Echeverria MG, Gorla DE, Marti GA. Modelling the potential geographic distribution of triatomines infected by Triatoma virus in the southern cone of South America. Parasites & Vectors. 2015;8:153.

26. Ceccarelli S, Balsalobre A, Medone P, Cano ME, Gurgel Gonçalves R, Feliciangeli D, et al. DataTri, a database of American triatomine species occurrence. Scientific Data. 2018;5:180071. doi:10.1038/sdata.2018.71.

bioRxiv preprint doi: https://doi.org/10.1101/738310; this version posted August 17, 2019. The copyright holder for this preprint (which was not certified by peer review) is the author/funder, who has granted bioRxiv a license to display the preprint in perpetuity. It is made available under aCC-BY-NC 4.0 International license.

27. Browne AJ, Guerra CA, Alves RV, Costa VMd, Wilson AL, Pigott DM, et al. The contemporary distribution of *Trypanosoma cruzi* infection in humans, alternative hosts and vectors. Scientific Data. 2017;4:170050. doi:10.1038/sdata.2017.50.

28. Barbet-Massin M, Jiguet F, Albert CH, Thuiller W. Selecting pseudo-absences for species distribution models: how, where and how many? Methods in Ecology and Evolution. 2012;3(2):327–338. doi:10.1111/j.2041-210X.2011.00172.x.

29. Warton DI, Shepherd LC. Poisson point process models solve the "pseudo-absence problem" for presence-only data in ecology. The Annals of Applied Statistics. 2010;4(3):1383–1402. doi:10.1214/10-AOAS331.

30. Renner IW, Elith J, Baddeley A, Fithian W, Hastie T, Phillips SJ, et al. Point process models for presence-only analysis. Methods in Ecology and Evolution. 2015;6(4):366–379. doi:10.1111/2041-210X.12352.

31. Phillips SJ, Dudík M, Elith J, Graham CH, Lehmann A, Leathwick J, et al. Sample selection bias and presence-only distribution models: implications for background and pseudo-absence data. Ecological Applications. 2009;19(1):181–197. doi:10.1890/07-2153.1.

32. Moyes CL, Shearer FM, Huang Z, Wiebe A, Gibson HS, Nijman V, et al. Predicting the geographical distributions of the macaque hosts and mosquito vectors of Plasmodium knowlesi malaria in forested and non-forested areas. Parasites & Vectors. 2016;9(1):242. doi:10.1186/s13071-016-1527-0.

33. Shearer FM, Longbottom J, Browne AJ, Pigott DM, Brady OJ, Kraemer MUG, et al. Existing and potential infection risk zones of yellow fever worldwide: a modelling analysis. The Lancet Global Health. 2018;6(3):e270–e278. doi:10.1016/S2214-109X(18)30024-X.

34. Fithian W, Elith J, Hastie T, Keith DA. Bias correction in species distribution models: pooling survey and collection data for multiple species. Methods in Ecology and Evolution. 2015;6(4):424–438. doi:10.1111/2041-210X.12242.

35. Vittinghoff E, McCulloch CE. Relaxing the Rule of Ten Events per Variable in Logistic and Cox Regression. American Journal of Epidemiology. 2007;165(6):710–718. doi:10.1093/aje/kwk052.

36. Concato J, Peduzzi P, Holford TR, Feinstein AR. Importance of events per independent variable in proportional hazards analysis I. Background, goals, and general strategy. Journal of Clinical Epidemiology. 1995;48(12):1495–1501. doi:10.1016/0895-4356(95)00510-2.

37. Peduzzi P, Concato J, Feinstein AR, Holford TR. Importance of events per independent variable in proportional hazards regression analysis II. Accuracy and precision of regression estimates. Journal of Clinical Epidemiology. 1995;48(12):1503–1510. doi:10.1016/0895-4356(95)00048-8.

38. Peduzzi P, Concato J, Kemper E, Holford TR, Feinstein AR. A simulation study of the number of events per variable in logistic regression analysis. Journal of Clinical Epidemiology. 1996;49(12):1373–1379. doi:10.1016/S0895-4356(96)00236-3.

39. Wan Z, Hook S. MOD11A2 MODIS/Terra Land Surface Temperature/Emissivity 8-Day L3 Global 1km SIN Grid V006. 2015;doi:10.5067/modis/mod11a2.006.

bioRxiv preprint doi: https://doi.org/10.1101/738310; this version posted August 17, 2019. The copyright holder for this preprint (which was not certified by peer review) is the author/funder, who has granted bioRxiv a license to display the preprint in perpetuity. It is made available under aCC-BY-NC 4.0 International license.

40. Lobser SE, Cohen WB. MODIS tasselled cap: land cover characteristics expressed through transformed MODIS data. International Journal of Remote Sensing. 2007;28:5079–5101.

41. Funk C, Peterson P, Landsfeld M, Pedreros D, Verdin J, Shukla S, et al. The climate hazards infrared precipitation with stations—a new environmental record for monitoring extremes. Scientific Data. 2015;2:150066. doi:10.1038/sdata.2015.66.

42. Lehner B, Verdin K, Jarvis A. New global hydrography derived from spaceborne elevation data. Eos, Transactions, American Geophysical Union. 2008;89(10):2. doi:10.1029/2008EO100001.

43. Jarvis A, Reuter H, Nelson A, Guevara E. CGIAR-CSI SRTM – SRTM 90m DEM Digital Elevation Database; 2008. Available from: `http://srtm.csi.cgiar.org/`.

44. M Friedl DSM. MCD12Q1 MODIS/Terra+Aqua Land Cover Type Yearly L3 Global 500m SIN Grid V006; 2015. Available from: `https://lpdaac.usgs.gov/node/1260`.

45. Weiss DJ, Atkinson PM, Bhatt S, Mappin B, I HS, W GP. An effective approach for gap-filling continental scale remotely sensed time-series. ISPRS Journal of Photogrammetry and Remote Sensing. 2014;98:106–118.

46. Esch T, Bachofer F, Heldens W, Hirner A, Marconcini M, Palacios-Lopez D, et al. Where we live—a summary of the achievements and planned evolution of the global urban footprint. Remote Sensing. 2018;10:10.

47. Savory DJ, Andrade-Pacheco R, Gething PW, Midekisa A, Bennett A, Sturrock HJW. Intercalibration and Gaussian Process Modeling of Nighttime Lights Imagery for Measuring Urbanization Trends in Africa 2000–2013. Remote Sensing. 2017;9(7):713. doi:10.3390/rs9070713.

48. Tatem AJ. WorldPop, open data for spatial demography. Scientific Data. 2017;4:170004. doi:10.1038/sdata.2017.4.

49. Weiss DJ, Nelson A, Gibson HS, Temperley W, Peedell S, Lieber A, et al. A global map of travel time to cities to assess inequalities in accessibility in 2015. Nature. 2018;553(7688):333–336. doi:10.1038/nature25181.

50. Heikkinen RK, Marmion M, Luoto M. Does the interpolation accuracy of species distribution models come at the expense of transferability? Ecography. 2012;35(3):276–288. doi:10.1111/j.1600-0587.2011.06999.x.

51. Wenger SJ, Olden JD. Assessing transferability of ecological models: an underappreciated aspect of statistical validation. Methods in Ecology and Evolution. 2012;3(2):260–267. doi:10.1111/j.2041-210X.2011.00170.x.

52. Trachsel M, Telford RJ. Technical note: Estimating unbiased transfer-function performances in spatially structured environments. Climate of the Past. 2016;12(5):1215–1223. doi:10.5194/cp-12-1215-2016.

53. Roberts DR, Bahn V, Ciuti S, Boyce MS, Elith J, Guillera-Arroita G, et al. Cross-validation strategies for data with temporal, spatial, hierarchical, or phylogenetic structure. Ecography. 2017;40(8):913–929. doi:10.1111/ecog.02881.

bioRxiv preprint doi: https://doi.org/10.1101/738310; this version posted August 17, 2019. The copyright holder for this preprint (which was not certified by peer review) is the author/funder, who has granted bioRxiv a license to display the preprint in perpetuity. It is made available under aCC-BY-NC 4.0 International license.

54. Wood SN. Fast stable restricted maximum likelihood and marginal likelihood estimation of semiparametric generalized linear models. Journal of the Royal Statistical Society: Series B (Statistical Methodology). 2011;73(1):3–36. doi:10.1111/j.1467-9868.2010.00749.x.

55. Kammann EE, Wand MP. Geoadditive models. Journal of the Royal Statistical Society: Series C (Applied Statistics). 2003;52(1):1–18. doi:10.1111/1467-9876.00385.

56. Wood SN. Generalized Additive Models: An Introduction with R. 2nd ed. Boca Raton: Chapman & Hall/Crc Texts in Statistical Science; 2017.

57. Marra G, Wood SN. Practical variable selection for generalized additive models. Computational Statistics & Data Analysis. 2011;55(7):2372–2387. doi:10.1016/j.csda.2011.02.004.

58. Wood SN, Li Z, Shaddick G, Augustin NH. Generalized Additive Models for Gigadata: Modeling the U.K. Black Smoke Network Daily Data. Journal of the American Statistical Association. 2017;112(519):1199–1210. doi:10.1080/01621459.2016.1195744.

59. Li Z, Wood SN. Faster model matrix crossproducts for large generalized linear models with discretized covariates. Statistics and Computing. 2019;doi:10.1007/s11222-019-09864-2.

60. Wood SN, Goude Y, Shaw S. Generalized additive models for large data sets. Journal of the Royal Statistical Society: Series C (Applied Statistics). 2015;64(1):139–155. doi:10.1111/rssc.12068.

61. R Core Team. R: A Language and Environment for Statistical Computing; 2018. Available from: `https://www.R-project.org/`.

62. Tennekes M. tmap: Thematic Maps in R. Journal of Statistical Software. 2018;84(1):1–39. doi:10.18637/jss.v084.i06.

63. Wickham H, François R, Henry L, Müller K. dplyr: A Grammar of Data Manipulation; 2019. Available from: `https://CRAN.R-project.org/package=dplyr`.

64. Wickham H, Henry L. tidyr: Easily Tidy Data with 'spread()' and 'gather()' Functions; 2019. Available from: `https://CRAN.R-project.org/package=tidyr`.

65. Valavi R, Elith J, Lahoz-Monfort JJ, Guillera-Arroita G. blockCV: An R package for generating spatially or environmentally separated folds for k-fold cross-validation of species distribution models. Methods in Ecology and Evolution. 2018;0(0). doi:10.1111/2041-210X.13107.

66. Richer W, Kengne P, Cortez MR, Perrineau MM, Cohuet A, Fontenille D, et al. Active dispersal by wild *Triatoma infestans* in the Bolivian Andes. Tropical Medicine & International Health. 2007;12(6):759–764. doi:10.1111/j.1365-3156.2007.01846.x.

67. Espinoza Echeverria J, Rodriguez AN, Cortez MR, Diotaiuti LG, Gorla DE. Spatial and temporal distribution of house infestation by *Triatoma infestans* in the Toro Toro municipality, Potosi, Bolivia. Parasites & Vectors. 2017;10(1):58. doi:10.1186/s13071-017-1984-0.

bioRxiv preprint doi: https://doi.org/10.1101/738310; this version posted August 17, 2019. The copyright holder for this preprint (which was not certified by peer review) is the author/funder, who has granted bioRxiv a license to display the preprint in perpetuity. It is made available under aCC-BY-NC 4.0 International license.

68. Bender A. Predictive maps of Chagas vectors; 2019. Available from: https://figshare.com/s/78e2c83427772ddd6cc9.

69. Grijalva MJ, Villacis AG, Moncayo AL, Ocana-Mayorga S, Yumiseva CA, Baus EG. Distribution of triatomine species in domestic and peridomestic environments in central coastal Ecuador. PLoS Neglected Tropical Diseases. 2017;11(10).

70. Rodríguez-Planes LI, Gaspe MS, Enriquez GF, Gürtler RE. Habitat-Specific Occupancy and a Metapopulation Model of *Triatoma sordida* (*Hemiptera*: *Reduviidae*), a Secondary Vector of Chagas Disease, in Northeastern Argentina. Journal of Medical Entomology. 2018;55(2):370–381. doi:10.1093/jme/tjx227.

71. Dorn PL, Monroy C, Curtis A. *Triatoma dimidiata* (Latreille, 1811): A review of its diversity across its geographic range and the relationship among populations. Infection, Genetics and Evolution. 2007;7(2):343–352. doi:10.1016/j.meegid.2006.10.001.

72. Bender A. Target-group background and spatial blocking for 30 triatomine species; 2019. Available from: https://figshare.com/articles/_/8604080/0.

73. Bender A. Visualization of predicted distribution of chagas vectors (with CI); 2019. Available from: https://figshare.com/articles/_/8617352/0.